Progress in Organic Coatings 187 (2024) 108165

Contents lists available at ScienceDirect

Progress in Organic Coatings

journal homepage: www.elsevier.com/locate/porgcoat

Molecular structure design of polybenzoxazines with low surface energy and low modulus for marine antifouling application

Jipeng Chen [a], Weibin Bai [b,*], Rongkun Jian [b], Yucai Lin [b], Xiaoxiao Zheng [a], Fangfang Wei [b], Qi Lin [a], Fengcai Lin [a,*], Yanlian Xu [a,*]

[a] Fujian Engineering and Research Center of New Chinese Lacquer Materials, College of Materials and Chemical Engineering, Minjiang University, Fuzhou 350108, China
[b] Fujian Key Laboratory of Polymer Materials, Fujian Provincial Key Laboratory of Advanced Oriented Chemical Engineering, College of Chemistry and Materials, Fujian Normal University, Fuzhou 350007, China

ARTICLE INFO

Keywords:
Marine antifouling
Polybenzoxazine
Low surface free energy
Low elastic modulus
Fouling release

ABSTRACT

The antifouling mechanism of low surface energy marine antifouling coatings is fouling release, and the key to fouling release is the adhesion strength of fouling organisms on the coating surface. Herein, we report an antifouling strategy to improve the fouling release performance of antifouling coatings by control the surface free energy and elastic modulus. Natural biomass cardanol-based benzoxazine monomers with different structures were designed by molecular structure and successfully synthesized via Mannich condensation. Detailed information of the chemical structure for the benzoxazines are analyzed by nuclear magnetic resonance (NMR) and Fourier transform infrared (FT-IR) spectroscopies. In addition, the benzoxazines polymerization behavior is investigated by differential scanning calorimetry (DSC) analyses. The properties such as surface free energy and elastic modulus of polybenzoxazine were adjusted by the structure of the amine source. Notably, polybenzoxazines with octadecylamine as amine source have higher contact angle and lower surface free energy, and their elastic modulus is significantly lower than that of the octylamine benzoxazine. The elastic modulus of the octylamine benzoxazine was 732.5 MPa, while that of octadecylamine benzoxazine was only 24.0 MPa. Therefore, the polybenzoxazine coating has less fouling adhesion and exhibits better fouling release performance, and thus has better antifouling properties. This non-releasing polybenzoxazines without antifouling agent is a green, eco-friendly antifouling coating with low surface energy and low elastic modulus designed by molecular structure.

1. Introduction

Marine biofouling is a global problem that causes huge economic losses and serious ecological problems for human maritime activities [1,2]. According to statistics, there are >4000 species of fouling organisms in the ocean [3,4], all of which attach themselves to the surface of underwater man-made structures and grow into marine biofouling, leading to a range of problems including increased fuel consumption [5], increased greenhouse gas emissions [6,7], aggravated equipment corrosion [8,9], and reduced aquaculture production [10]. Marine biofouling is therefore a pressing issue. Among many antifouling strategies, the application of marine antifouling coatings is the simplest, most economical and effective antifouling strategy [11]. However, traditional antifouling coating usually contains a large amount of antifouling agent, which is released into the marine environment, killing the fouling organisms and at the same time seriously endangering the marine ecosystem, and causing secondary pollution [11–13]. On the other hand, the release of microplastics from traditional antifouling coating is another serious environmental concern [2]. Paint particles have long been reported to be one of the major sources of neglected microplastics in the marine environment [14]. Fortunately, the release of microplastics from marine antifouling paints has recently attracted the attention of researchers and become a hot topic. Therefore, the development of marine antifouling coatings that do not contain antifoulant and do not release microplastic is an effective strategy to solve these environmental problems.

Fouling release coating (FRC) with low surface energy is a marine antifouling coating that does not release antifouling agents [15]. It is typically based on a structurally stable, non-hydrolysable silicone or organofluoride polymer matrix and therefore does not release

* Corresponding authors.
E-mail addresses: bai-wb@fjnu.edu.cn (W. Bai), fengcailin@mju.edu.cn (F. Lin), ylxu@mju.edu.cn (Y. Xu).

https://doi.org/10.1016/j.porgcoat.2023.108165
Received 6 November 2023; Received in revised form 6 December 2023; Accepted 17 December 2023
Available online 2 January 2024
0300-9440/© 2023 Elsevier B.V. All rights reserved.

antifouling agents or microplastics into the marine environment, making it a green and eco-friendly antifouling technology [3,16]. FRCs typically have extremely smooth surface and quite low surface energy. As a result, FRCs reveal minimized adhesion strength for fouling organisms, so that microorganisms can only adhere very weakly to the coated surface [5]. FRCs consequently capacitate the easy removal of surface-adhered organisms by water flow during the ship navigation to achieve fouling release. Therefore, the antifouling performance of FRCs depends on the adhesion of the fouling organisms to the coating surface, and the weaker the adhesion of the fouling organisms, the better the antifouling performance [17]. The adhesion strength of fouling organisms to the surface of FRCs is related to the surface free energy and modulus of the coating, and the magnitude of the adhesion is positively correlated to the surface free energy and modulus [18,19]. The lower the surface energy and modulus, the weaker the adhesion of fouling organisms to the coating, and the easier it is to remove, giving better fouling release performance. However, the organosilicon polymers are bonded to the substrate via van der Waals interactions, resulting in poor substrate adhesion [20,21]. In addition, organoflouorine polymer have problems such as high rigidity, high modulus and difficult to process [22]. The inherent shortcomings of FRC polymers limit the application of FRC in marine antifouling [23].

Polybenzoxazine is a new type of thermosetting phenolic resin with unlimited potential [24]. Due to excellent properties, i.e., low flammability [24,25], high glass transition temperature [26,27], high thermal stability [28,29], low dielectric constant [30,31], low surface energy [17,32] and excellent adhesion properties [15,33], polybenzoxazine has a wide range of applications in electronics, composites, coatings and adhesives [34–36]. Benzoxazine resins have good film-forming and mechanical properties, and their unique chemical structures contain a large number of intra- and intermolecular hydrogen bonds [37]. The presence of hydrogen bonds reduces the surface free energy of polybenzoxazine, benzoxazine polymers thus become a new type of non-silicone and non-fluorine low surface energy material with excellent performance, and its surface free energy is even lower than that of polytetrafluoroethylene (PTFE) [38]. On the other hand, the hydrogen bonding force is much larger than the van der Waals force, which can improve the substrate adhesion and give polybenzoxazine good bonding properties. Our previous work reported a urushiol-based benzoxazine copper polymer (UBCP) for marine antifouling coatings application, the UBCP coating has outstanding antifouling performance combined with low surface energy and strong substrate adhesion [17]. In addition, molecular designability modulates the modulus of polybenzoxazine by introducing different long flexible alkyl chains to design low surface energy and low modulus benzoxazine polymer coatings. Therefore, polybenzoxazine is expected to be used as a novel low surface energy FRC matrix to modulate the surface free energy and modulus to obtain outstanding fouling release performance meanwhile solving the inherent poor substrate adhesion of FRC.

Cardanol (CA), as a major component by vacuum distillation of cashew nut shell liquid, is a natural bio-based phenol with a unique unsaturated 15-carbon long side chain alkane that has attracted attention for a wide range of applications in resins, coatings, surfactants and organic synthesis in recent decades, CA has also been used as a green and renewable biomass phenol for the development of eco-friendly bio-based benzoxazine [39–43]. Notably, nanomaterials were introduced into cardanol/stearylamine based benzoxazine to prepare nanocomposite systems with superhydrophobic, corrosion-resistant and low dielectric features [44–46]. Nevertheless, in view of the molecular structure of cardanol/stearylamine based benzoxazine has many outstanding properties and shows great potential for applications. The component of CA are themselves mixtures of four different saturations in the side chain (Scheme 1), namely saturated (5–8 %), monoene (48–49 %), diene (16–17 %) and triene (29–30 %) [47]. It can be used to modulate the modulus of benzoxazine polymers and in conjunction with an amine source with long flexible alkyl chains, which will effectively

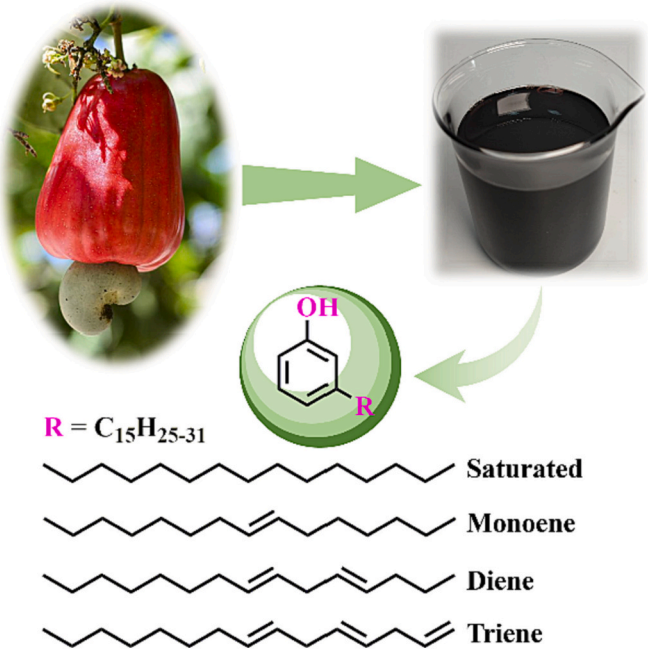

Scheme 1. Cashew fruit and components of cardanol.

reduce the modulus of benzoxazine polymers. Moreover, the long unsaturated side chains provide active sites to enhance the cross-linking of the benzoxazine polymer, which in turn improve the polymer's properties. Cardanol-based benzoxazine resins with low surface energy and low modulus and excellent properties for combating marine biofouling thus will be developed. Based on the above, this work will design different structures of benzoxazine by molecular structure design, using CA as the main phenolic source with different carbon chains of primary amines. Subsequently, the benzoxazine polymer coatings were prepared by ring-opening polymerization under heating. The hydrophobicity, surface free energy, and elastic modulus of benzoxazine polymer coatings will be modulate by adjusting the structures of phenolic and amine sources. The fouling release performance was then systematically evaluated using typical fouling organisms, i.e., the bacteria *Escherichia coli* (*E. coli*), *Staphylococcus aureus* (*S. aureus*) and the marine bacterium *Vibrio alginolyticus* (*V. alginolyticus*) as well as marine microalgae species *Nitzschiaclosterium* (*N. closterium*), *Phaeodactylumtricornutum* (*P. tricornutum*) and *Dicrateriazhanjiangensis* (*D. zhan-jiangensis*) to investigate the antifouling performance of benzoxazine polymer coatings. The major purpose of this work is to provide a theoretical and experimental basis for the development of a novel, green, eco-friendly and low surface energy FRC marine antifouling technology without antifoulant release and microplastic release.

2. Materials and methods

2.1. Materials

Analytical grade paraformaldehyde, 1,4-dioxane, dichloromethane, xylene, ethanol and anhydrous sodium sulfate were purchased from Sinopharm Chemical Reagent Co. Ltd. (Shanghai, China). *n*-Octylamine and Octadecylamine was purchased from Shanghai Macklin Biochemical Co., Ltd. (China). Unless otherwise specified, all chemicals were analytical grade reagents and were used as received without further purification. Cardanol (CA) was purchased from Fujian Jianyang Xinhua Chemical Co., Ltd. (Nanping, China). Deionized (DI) water was purified by a Lab pure water system (WP-RO-10B) from Sichuan Wortel Water Treatment Equipment Co., Ltd. (China) and was used throughout the work. Phosphate-buffered buffered saline (PBS, pH = 7.4) was

purchased by Shanghai Sangon Biotech Co., Ltd. (Shanghai, China). Artificial seawater (ASW) was prepared according to ASTM D1141-1998 (2013). *Escherichia coli* (*E. coli*), *Staphylococcus aureus* (*S. aureus*) and *Vibrio alginolyticus* (*V. alginolyticus*) were purchased from BeNa Chuanglian Biotechnology Co., Ltd. (Shangcheng, Henan province, China). *Nitzschiaclosterium* (*N. closterium*) *Phaeodactylumtricornutum* (*P. tricornutum*) and *Dicrateriazhanjiangensis* (*D. zhan-jiangensis*) were purchased from Seaweed Culture Collection Center, Institute of Oceanology, Chinese Academy of Sciences (Qingdao, China).

2.2. Preparation of cardanol-based benzoxazine monomers (CB)

Cardanol-based benzoxazine monomers (CB) was prepared using previously established procedure [17,48]. Briefly, paraformaldehyde (0.15 mol, 4.50 g) was loaded in a 250 mL three-necked round bottom flask equipped with a thermometer, a reflux condenser and a dropping funnel. Then, *n*-octylamine (0.05 mol, 6.46 g) and 1,4-dioxane (20 mL) were added to the flask, and the mixture was stirred at room temperature for 40 min cardanol (0.05 mol, 15.00 g) was dissolved in 1,4-dioxane (20 mL), and added dropwise to the reaction system within 20 min. Subsequently, the system was gradually heated to 90 °C, and kept for 5 h under vigorous stirring. Afterwards, the system was cooled down to room temperature, and the solvent was removed by vacuum distillation. The residual mixture was dissolved in dichloromethane (100 mL), and the solution was washed with deionized (DI) water for three times, followed by drying with anhydrous sodium sulfate overnight. Finally, the solvent was removed by rotary evaporation, and reddish-brown viscous product was obtained, which was dried under vacuum at room temperature for 24 h and was named as COB.

In the same way, cardanol (0.05 mol, 15.00 g), paraformaldehyde (0.15 mol, 4.50 g) and octadecylamine (0.05 mol, 13.48 g) were also used to synthesize another cardanol-based benzoxazine monomers, which was named as CDB.

2.3. Fabrication of cardanol-based benzoxazine polymer coatings

The curing reaction for COB and CDB polymer coatings were prepared as the following procedure: a certain amount of benzoxazine monomer and xylene were loaded in a beaker and stirred until a homogeneous solution (40 wt%) was obtained. The solution was cast onto glass slides (for surface wettability, bacteria-resistant assay and algal inhibition assay), polished tinplates (for flexibility, hardness and adhesion). Bare glass slides (BG, 2.5 cm × 2.5 cm) and polished tinplates (5.0 cm × 2.5 cm and 12.0 cm × 2.5 cm) were cleaned by ultrasonication for 10 min sequentially using acetone, ethanol and DI water, and then dried under flowing N_2 to remove any contaminants. The solution first cured at ambient temperature for 1 h for allow the evaporation of solvent and then step-cured in a convection oven for 1 h at 100 °C, 1 h at 120 °C, 1 h at 140 °C, 1 h at 160 °C, and 1 h at 180 °C. Once they were completely cured, the samples were allowed to slowly cool to room temperature, and the dark brown films were obtained. For convenience, the coatings were designated as COHP and CDHP. The coatings have an average thickness of ca. 60 μm, determined by a Qnix® 4500 coating thickness gauge (Qnix, Germany), according to ASTM B499-2009 (2014).

2.4. Characterizations

The chemical structure of CB samples was confirmed by attenuated total reflectance Fourier transform infrared (ATR-FTIR) and ^{1}H NMR spectra. ATR-FTIR spectra was recorded on a Nicolet 5700 FTIR spectrometer (Thermo Fisher, USA) in the range of 400–4000 cm^{-1}. ^{1}H NMR spectra was recorded on a Bruker 400 MHz NMR spectrometer (Bruker, Germany), using $CDCl_3$ as the solvent. The thermal stability of benzoxazine monomers and polybenzoxazine coatings was performed on a METTLER TGA2 thermal analyzer (Mettler-Toledo, Switzerland) from 30 to 600 °C at a heating rate of 10 °C·min^{-1} under nitrogen atmosphere. The curing behavior of benzoxazine monomers was analyzed by differential scanning calorimetric (DSC) measurement conducted on a DSC2500 (TA, USA) from 30 to 280 °C at different heating rate under nitrogen atmosphere. The water contact angle (WCA) was determined by a drop shape analyzer DSA 25 instrument (Kruss, Germany) using a 2 μL DI water droplet at ambient temperature. The surface free energy (SFE) was determined according to the EOS model. The average WCA and SFE value of each sample was calculated by averaging five data points. The droplet adhesion force on the coatings surface was measured by a force tensiometer K100MK2 instrument (Kruss, Germany) using a 6 μL DI water droplet at an immersion depth of 0.1 mm and immersion time of 0.01 min at ambient temperature, and each sample was measured for five times to obtain the average value. Dynamic mechanical analyses (DMA) were performed on the specimens with the size of 15 × 10 × 0.06 mm^3 through TA Q800 apparatus (TA, USA) from 30 to 200 °C at a heating rate of 5 °C/min with film tension mode, the frequency was set as 1.0 Hz, and the oscillation amplitude was fixed at 5.0 μm. Tensile tests were performed with a constant rate of 5 mm/min on a ETM104B universal testing machine (Wance Testing Machine Co., Ltd. Shenzhen, China) according to GB/T 1040.3–2006 standard. The rectangular samples with the dimension of 75 × 20 × 0.05 mm^3 were used for tensile tests.

2.5. Antibacterial assessments

The antibacterial performance of the polybenzoxazone coatings was evaluated using two typical bacteria−Gram-negative *E. coli* BW25113 and Gram-positive *S. aureus* ATCC 25923 and the marine bacterial species *V. alginolyticus* ATCC 33787 according to the previous procedure. The freezing stocks of *E. coli* and *S. aureus* bacterial strains were maintained at −80 °C in 1:1 solution of Luria-Bertani (LB) broth: 40 % (v/v) glycerol. Prior to use in antibacterial tests, the bacterial strains were first cultured in fresh LB broth at 37 °C by shaking at 170 rpm for 20 h, until the $O.D._{600nm}$ of 1.8–2.0 was reached. The *V. alginolyticus* was stored frozen at −80 °C in solution of 2216E medium and glycerol, similarly, preactivated in fresh 2216E medium at 30 °C. Then, BG and polybenzoxazone coatings (7.5 cm × 2.5 cm) were cleaned by wiping with anhydrous ethyl alcohol, sterilized with ultraviolet radiation for 30 min, and placed in plastic petri dishes. The suspensions of bacteria were diluted to ca. 10^5–10^6 CFU/mL in fresh medium, determined using a hemocytometer (Shanghai Qiujing Biochemical Reagent Instrument Co. Ltd., China). Subsequently, BG and polybenzoxazone coatings were inoculated with 500 μL of diluted bacterial suspension and covered with plastic wraps. The bacterial strains were incubated at 37 °C (*E. coli* and *S. aureus*) and 30 °C (*V. alginolyticus*) for 24 h under static condition. Afterwards, the plastic wraps were removed and the plates were gently rinsed with 20 mL of sterile phosphate-buffered saline (PBS) to ensure that non-adhered bacteria were washed away. The washed bacteria were cultured on agar plates, and the number of colonies was counted. To quantify the number of surface-adhered bacteria, the washed BG and polybenzoxazone coatings were examined by FE-SEM (Phenomenon, Netherlands).

2.6. Algal biofouling assessments

To evaluate the effects of polybenzoxazone coatings on algae, algal growth and attachment experiments were conducted. Algal cells *N. closterium*, *P. tricornutum* and *D. zhan-jiangensis* cells were grown in f/2 culture media, which were prepared in ASW at 22 ± 2 °C under a cycle of 12 h of fluorescent light and 12 h of dark. After 7 days of growth, the culture media containing algal cells were diluted with fresh culture media to give the test media with the concentrations of algal cells at 10^5–10^6/mL, which were used for the following algal attachment experiments.

Similar to the antibacterial assessments, the sterilized BG and polybenzoxazone coatings were immersed in glass petri dish containing 30

mL of culture media inoculated with *N. closterium*, *P. tricornutum* and *D. zhan-jiangensis* cells. After immersed for 1 day, 3 days, 5 days and 7 days, the concentrations of *N. closterium*, *P. tricornutum* and *D. zhan-jiangensis* cells were determined by counting the number of cells using a hemocytometer (Shanghai Qiujing Biochemical Reagent Instrument Co. Ltd., China), and the optical photographs of algal growth process were recorded. After settling down, BG and polybenzoxazone coatings were taken out from the test media, and rinsed with 20 mL of sterile PBS to wash away any non-adhered algae. Subsequently, the algae adhered onto the surfaces of BG and polybenzoxazone coatings were examined using a fluorescence microscope (Eclipse Ci-L plus, Nikon, Japan), and the images of five random fields (20× magnification, 0.156 mm^2/per field) were recorded for each sample. The algal coverage over BG and polybenzoxazone coatings was determined by analyzing the fluorescence microscope images using the ImageJ software.

3. Results and discussion

3.1. Synthesis and characterization of CB monomers

A large number of benzoxazine monomers and their corresponding polymers (after thermal curing polymerization) have been reported that the flexible and simple molecular design of benzoxazine resins. In this study, based on flexible molecular design, a series of bio-based phenolic benzoxazines were designed and synthesized. Cardanol was used as phenol sources, octylamine and octadecylamine as amine sources, which were combined with paraformaldehyde for the Mannich condensation to prepare benzoxazine monomers and named as COB and CDB, as shown in Fig. 1a. Subsequently, the corresponding polybenzoxazines were obtained by thermal curing and ring-opening polymerization (ROP). The presence of the oxazine ring in the COB and CDB structures were confirmed by using ATR-FTIR spectroscopy, ^{1}H NMR spectroscopy, and differential scanning calorimetry (DSC). Urushiol-based benzoxazine (UB) was used as a verification experiment, and the synthesis and structural characterization of UB are shown in Supporting Information.

The ATR-FTIR spectra of CA, COB and CDB (Fig. 1b) featured absorption bands centered at 3347.5, 3012.6, 2927.2 and 2853.4 cm^{-1} representing free phenolic –OH, =C–H and C—H stretching vibrations. In addition, the absorption peaks at 1586.0 cm^{-1} and 1455.5 cm^{-1} are assigned to C=C stretching vibrations. The spectra of COB and CDB contained absorption bands at 1240.2 cm^{-1} for the symmetric stretching vibrations, respectively, of the Ar – O – C unit in the oxazine ring [44,46]. The asymmetric stretching modes of the C – N – C bond in the oxazine ring of the benzoxazine ring appeared at 1122.0 and 1121.0 cm^{-1} [49,50]. Moreover, the characteristic oxazine ring-related band occurred at 965.2 and 964.7 cm^{-1} for COB and CDB respectively. Afterwards, the ^{1}H NMR spectra of C and the newly synthesized benzoxazine monomers (CB) were also compared in $CDCl_3$ (Fig. 1c). Obviously, two single peaks were observed in the ^{1}H NMR spectra of CB at 3.95 and 4.84 ppm, and the integrated area ratio was approximately 1:1, which were ascribed to the protons of Ar–CH_2–N and O–CH_2–N in the oxazine ring of benzoxazine monomers, respectively. These results illustrate the successful synthesis of CB.

3.2. Thermal behavior of CB monomers

The newly synthesized CB monomers were thermally cured to obtain the corresponding polybenzoxazines, and the thermal ROP behavior of CB monomers was investigated by ATR-FTIR, TGA, and DSC. To monitor the structural transformations of polybenzoxazines after thermal ROP, ATR-FTIR spectral measurement was performed. The ATR-FTIR of polybenzoxazines was shown in Fig. 1b. The characteristic oxazine ring absorption band, which occurred at 965.2 and 964.7 cm^{-1} for COB and CDB, respectively, 1240.2 cm^{-1} (C – O – C symmetric stretching) was not present in the ATR-FTIR spectra of COHP and CDHP. Notably, the characteristic absorption peak at 3300 cm^{-1}– 3400 cm^{-1} with significantly enhanced intensities in the ATR-FTIR spectra of polybenzoxazines after thermosetting, which caused by the presence of freer phenolic –OH and formed a lot of hydrogen bonds. These results suggesting that the oxazine ring in the benzoxazine moiety had undergone ROP to form a cross-linked and more thermally stable polybenzoxazine.

TGA profiles were recorded to investigate the thermal stability (in terms of the initially decomposes temperature ($T_{5\%}$, which defined as the temperature for 5 wt% decomposition) and char yield) of benzoxazine before and after thermal curing polymerization, and the results are shown in Fig. 2 and Table 1. It is found that the uncured benzoxazines monomer initially decomposes at 160.5 °C and 224.3 °C, and in the end of test, the residue of 6.5 wt% and 10.7 wt% is left for COB and CDB, respectively. After thermal curing, the thermal stability of newly obtained polybenzoxazines had increased dramatically relative to that of

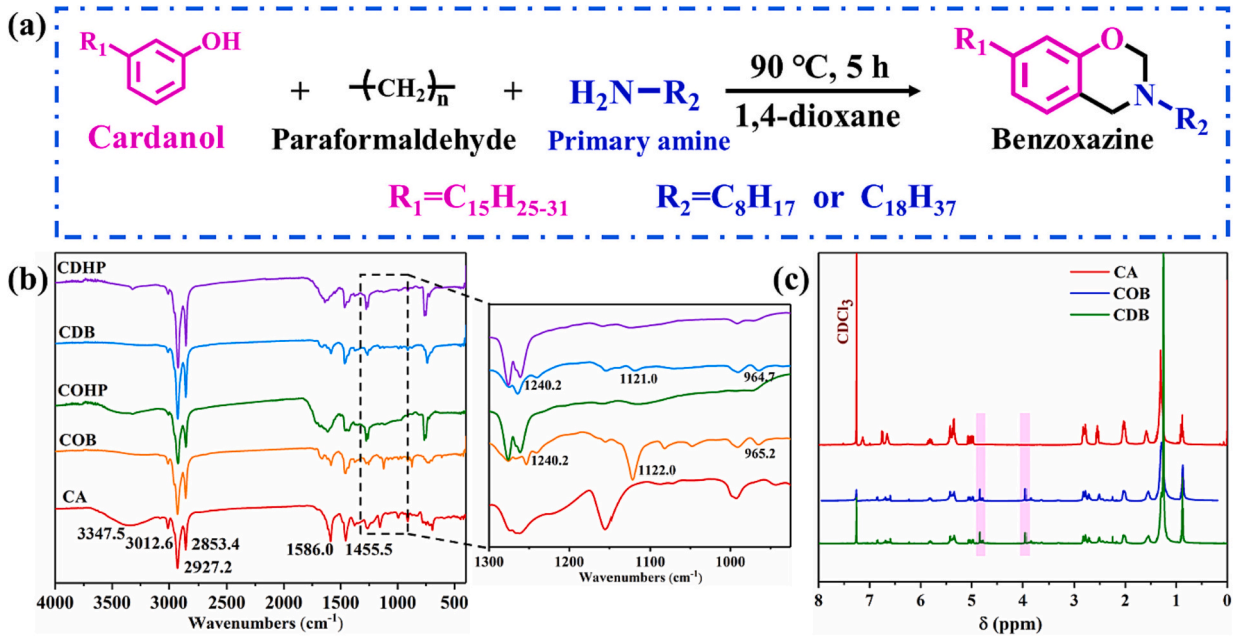

Fig. 1. (a) Syntheses of the CB monomers, (b) ATR-FTIR spectra of CA, COB, CDB, COHP and CDHP, (c) ^{1}H NMR spectra of CA and CB monomers.

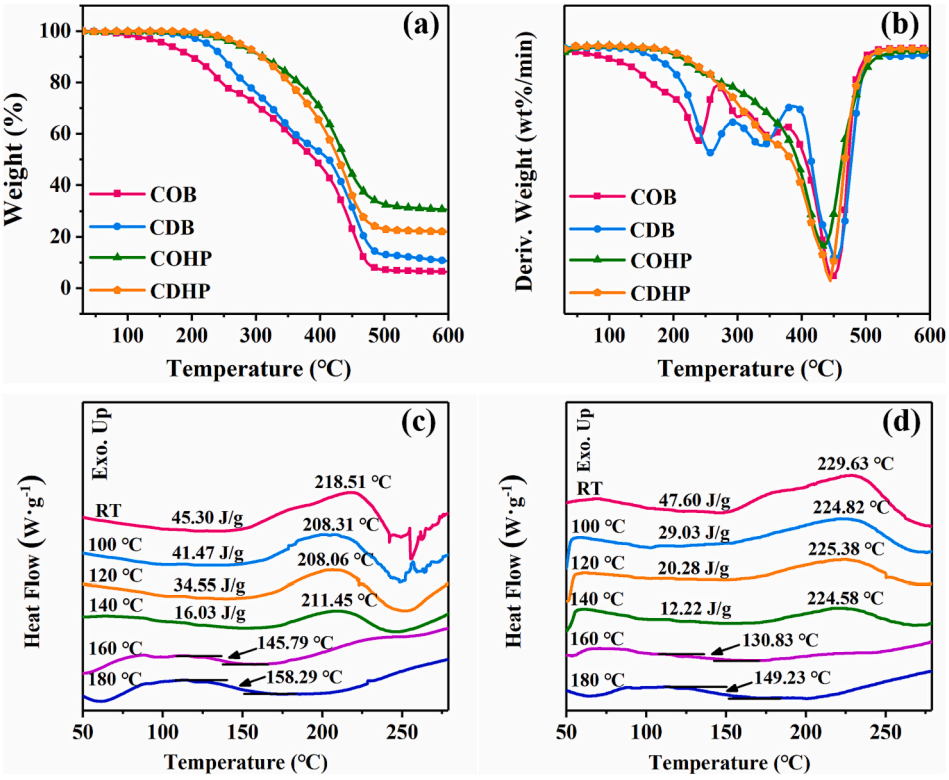

Fig. 2. TGA (a) and DTG (b) curves of COB, CDB, COHP and CDHP. DSC thermogram of (c) COB and (d) CDB after different temperature treatment.

Table 1
Thermal-stability parameters of COB, CDB, COHP and CDHP derived from TGA and DTG curves.

Samples	$T_{5\%}$ (°C)	T_{max} (°C)	Residue at 600 °C (wt%)
COB	160.5	448.5	6.5
CDB	224.3	455.7	10.7
COHP	268.3	432.8	30.7
CDHP	276.3	444.3	22.0

the uncured sample. The value of $T_{5\%}$ increased to 268.3 °C and 276.3 °C, and the residue increased to 30.7 wt% and 22.0 wt% for COHP and CDHP, respectively. Obviously, these results caused by the complete ROP of the benzoxazine monomers and cross-linking of long side chains resulted in the formation of a more stable structure that displayed improved thermal stability.

The DSC thermogram of the uncured CB monomers in Fig. 2c and d revealed a visible thermal event: a maximum exothermic curing peak. The exothermic curing peak, at 218.51 °C and 229.63 °C for COB and CDB, respectively, can be attributed mainly to opening of the oxazine ring in benzoxazine monomers and the formation of corresponding polymeric product, COHP and CDHP, respectively, at this higher temperature. Notably, the maximum exothermic curing peak of UB (see Fig. S4) is much lower than that of CB, which caused by the latent catalytic effect from the presence of a phenolic hydroxyl group on UB structures [51]. Moreover, it is evident that the polymerization enthalpy of UB was much higher than CB. Such a high heat release during the polymerization process is possibly attributed from the multiple polymerization mechanisms including the ROP of oxazine ring and cross-linking of long side chains, while it is clear that the side chains of urushiol have more active sites than cardanol [51]. Furthermore, after thermal treatment of each benzoxazine monomer at 100 °C, the maximum exothermic peaks shifted to lower temperatures (208.31 and 224.82 °C for COB and CDB, respectively). This behavior indicated that the structure of benzoxazine monomers had changed after thermal treatment, such as molecular segments no longer freeze and segmental motion become more easily, with the structural transformation and segmental motion also affecting its ROP process. When the temperature of thermal treatment increased to 140 and 160 °C, the exothermic peak of UB disappeared completely indicating that completion of the ROP, and a glass transition temperature (T_g) was observed, which indicates the excellent thermal property of the final thermoset. However, the exothermic peak of CB disappeared completely was observed at 160 and 180 °C and the T_g of CB was significantly higher than that of UB, which ascribe to differences in the structure of urushiol and cardanol. On the one hand, the latent catalytic effect from the presence of a phenolic hydroxyl group on UB structures, which reduced the ROP temperature of UB. On the other hand, the presence of phenolic hydroxyl groups also leads to more intramolecular hydrogen bonds and reduces intermolecular hydrogen bonds, while CB has more intermolecular hydrogen bonds after thermosetting, which increases the degree of cross-linking and thus increases T_g [52,53]. The T_g of UOB is higher than that of UDB, and that of COB is higher than that of CDB, which is due to the existence of long and flexible octadecylamine structures in UDB and CDB. The carbon chain of octadecylamine is longer, which leads to greater flexibility. The increase in flexibility is enough to compensate for the volume effect, which increases the distance between molecular segments, weakens the interaction force, and produces internal plasticization.

The activation energy (E_a) for the ROP of newly designed benzoxazine monomers was also investigated with non-isothermal DSC at different heating rates of 2, 5, 10, 15 and 20 °C/min. The DSC thermograms of benzoxazine monomers at different heating rates were shown in Fig. 3. Then, the value of E_a for the ROP process was determined via the well-known Kissinger and Ozawa methods. Based on the Kissinger and Ozawa methods, the value of E_a can be calculated by the following equations:

$$ln\left(\frac{\beta}{T_P^2}\right) = ln\left(\frac{AR}{E_a}\right) - \frac{E_a}{RT_P} \quad \text{Kissinger equation} \tag{1}$$

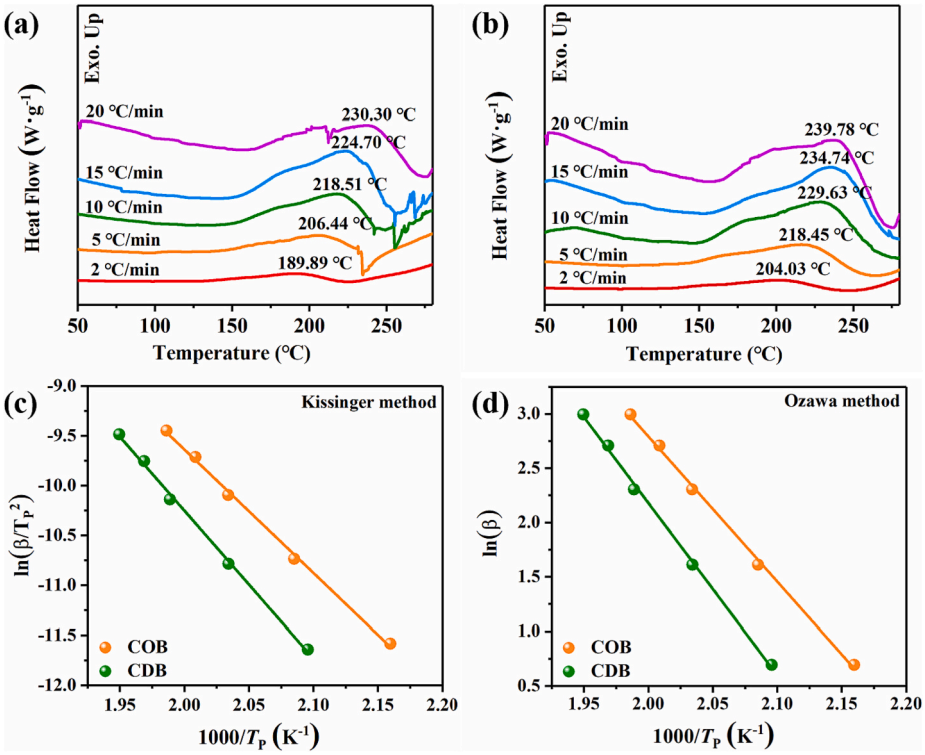

Fig. 3. Kinetic thermal curing behavior of COB (a), and CDB (b) at various heating rates through DSC measurements. (c) Representations of the Kissinger and Ozawa method for the calculation of the activation energy (E_a) of COB and CDB.

$$ln\beta = -1.052\frac{E_a}{RT_P} + C \quad \text{modified Ozawa equation} \tag{2}$$

where β is the heating rate, T_P is the thermodynamic temperature at the exothermic peak maximum, A is the pre-exponential factor, R is the gas constant, and C is a constant. When the heating rate was 20 °C/min, the polymerization temperatures of COB and CDB were 230.30 and 239.78 °C; at 15, 10, 5 and 2 °C/min, the polymerization temperatures of COB were 224.70, 218.51, 203.44 and 189.89 °C, and that of CDB were 234.74, 229.63, 218.45 and 204.03 °C, respectively (Fig. 3a and b). As shown in Fig. 3c, the plots exhibit straight lines based on the two theories for the newly designed benzoxazine monomers and the values of E_a were summarized in Table 2. The E_a values calculated from the slope of Kissinger and Ozawa's plots for COB are 103.01 and 105.58 kJ/mol, and that of CDB are 123.30 and 125.03 kJ/mol, respectively. Notably, previously reported value of E_a for the benzoxazine monomer were 247 and 250 kJ/mol when calculated by using the Kissinger method or Ozawa methods, respectively. This kinetic analysis confirmed that when compared with the traditional benzoxazine monomer structure, the newly designed bio-based COB and CDB could more readily undergo ROP, without consuming too much energy. In comparison, the E_a values of UOB and UDB are obtained to be 96.11, 98.63 kJ/mol and 94.86, 97.44 kJ/mol (see Fig. S5 and Table S1), respectively. Obviously, the E_a values of UB are lower than that of CB, regardless of the Kissinger method or Ozawa method. This kinetic analysis confirmed that The UB could more readily undergo ROP at a lower temperature, without consuming too much energy, which attributed to the latent catalytic group (–OH) present in the benzoxazine structure result from the differences in the structure of urushiol and cardanol.

Table 2
The activation energy of COB and CDB obtained by Kissinger and Ozawa methods.

Samples	Kissinger		Ozawa	
	Linear fit equation	E_a (kJ·mol^{-1})	Linear fit equation	E_a (kJ·mol^{-1})
COB	y = 15.15–12.39x	103.01	y = 29.51–13.36x	105.58
CDB	y = 19.41–14.83x	123.30	y = 33.82–15.82x	125.03

On the basis of the relevant literatures [54,55], generally, the ROP process of benzoxazine follows a self-catalytic polymerization mechanism, which must be achieved at high temperature (>200 °C). Scheme 2 provides a suggested mechanism for the transformation of CB during the ROP process, according to the DSC and FTIR spectral data. As shown in Scheme 2, after thermal treatment, the cleavage of O–CH_2–N in the CB oxazine ring due to the gain of energy, then the cationic moieties of zwitterionic intermediates were formed. The other benzoxazine monomers attacked the cationic imine moieties though electrophilic substitution. Consequently, the structure was rearranged to form a new type of Mannich bridge. Finally, the oxazine ring in the benzoxazine underwent ROP under continuous heating to form a cross-linked polymer. At the same time, the unsaturated bonds on the side chains of urushiol and cardanol are further cross-linked, affording UOHP, UDHP, COHP and CDHP as a highly cross-linked network, respectively. Furthermore, as a lot of –OH and N exist in the highly cross-linked network, forming a large number of intermolecular and intramolecular hydrogen bonds (Scheme 2), which in turn affects the property of UOHP, UDHP, COHP and CDHP such as T_g.

In order to explore crosslinking density (ρ) after the ROP of polybenzoxazines (COHP, CDHP, UOHP and UDHP) in this work and the storage modulus (E') of the newly designed polybenzoxazines with different structures, the DMA of polybenzoxazines was performed, and shown in Fig. 4. The crosslinking density (ρ) can be obtained from a statistical theory of rubbery elasticity theory according to Eq. (3):

$$\rho(E') = \frac{E'}{3\Phi RT} \tag{3}$$

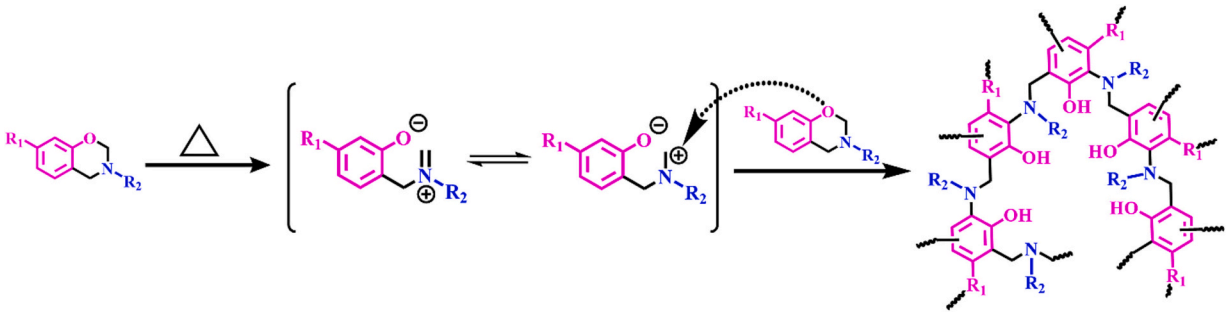

Scheme 2. Suggested mechanism of the transformation of CB after ROP.

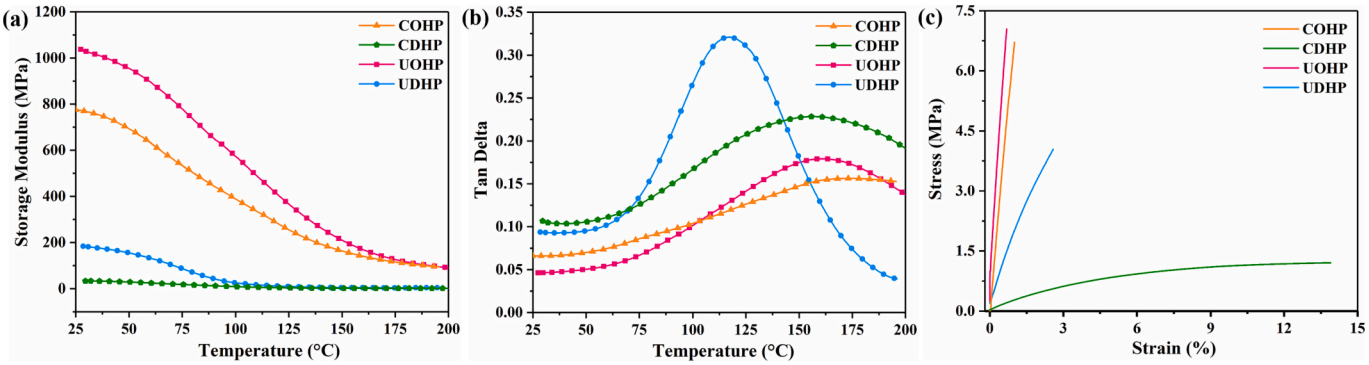

Fig. 4. (a) The storage modulus and (b) tan delta vs. Temperature of polybenzoxazine coatings. (c) (c) the stress-strain curves of polybenzoxazine coatings.

where E' is the storage modulus at 30 K above T_g, Φ is the front factor, which is 1 here, R is the gas constant, and T is the thermodynamic temperature at T_g + 30 °C. The crosslink density of polybenzoxazines (COHP, CDHP, UOHP and UDHP) was calculated and shown in Table 3. Although the chains of polybenzoxazines were significantly restricted by hydrogen bonds in the glassy state, hydrogen bonds were very weak above T_g. Therefore, crosslink density can be calculated accurately at 30 K above T_g. As can be seen, the storage modulus (E') of COHP, CDHP, UOHP and UDHP at T_g + 30 K were 94.51, 1.36, 99.22 and 4.83 MPa, respectively. In addition, the crosslink density (ρ) of COHP, CDHP, UOHP and UDHP were 8.0×10^3, 0.12×10^3, $8.56 \times 10^3$and 0.46×10^3, respectively. As shown in Fig. 4a and Table 3, the E' of COHP, CDHP, UOHP and UDHP at 30 °C were 767.66, 33.49, 1027.73 and 182.75 MPa respectively. It is clear that the E' of CDHP and UDHP at 30 °C is much lower than that of COHP and UOHP. Significantly decreased E' illustrates the improved flexibility of CDHP and UDHP.

Besides, mechanical properties related to tensile parameters were also tested. As seen in Fig. 4c and Table 3, COHP and UOHP display the similar behavior during the tensile testing, after fracture, COHP gets a tensile strength of 6.80 MPa and elongation at break of 1.01 %, while that values for UOHP are 7.13 MPa and 0.69 %, which display the strong rigidity of COHP and UOHP. While the slope of the stress-strain curve of UDHP is lower than that of COHP and UOHP possibly due to the lower rigidity of UDHP, and the tensile strength decreases and the elongation at break increases, the value is 4.06 MPa and 2.06 %, respectively. Notably, the slope of the stress-strain curve and tensile strength of CDHP decreased sharply, while the elongation at break increased significantly, indicating that CDHP has the best flexibility and the lowest elastic modulus. Compared with COHP and UOHP, CDHP and UDHP have lower elastic modulus, which is consistent with the DMA test results.

These results of mechanical properties are mainly due to the introduction of long and flexible octadecylamine into the CDHP and UDHP structure. The carbon chain of octadecylamine is longer, which leads to greater flexibility. The increase in flexibility is enough to compensate for the volume effect, which increases the distance between molecular segments, weakens the interaction force, and produces internal plasticization. Furthermore, the modulus of UOHP is higher than that of COHP, and the modulus of UDHP is higher than that of CDHP, which is mainly due to the cross-linking density in the polybenzoxazine molecule. Higher crosslink density restricts the movement of molecular segments, which in turn leads to higher modulus. Low modulus predicts higher potential fouling release performance. In addition, in the DMA test, the T_g of COHP and CDHP is higher than that of UOHP and UDHP, and the T_g of UOHP is higher than that of UDHP, and the T_g of COHP is higher than that of CDHP. These results are consistent with the DSC test results, which are attributed to hydrogen bonding and long, flexible carbon chain influence.

3.3. *Surface properties of polybenzoxazine coatings*

The WCA and SFE was adopted to study the hydrophobicity and surface energy of the newly designed polybenzoxazine coatings, the

Table 3
Mechanical properties parameters of COHP, CDHP, UOHP and UDHP coatings.

Samples	E' at 30 °C (MPa)	T_g at the max Tan Delta (°C)	E' at (T_g + 30 K) (MPa)	ρ ($\times 10^3$ mol·m^{-3})	Tensile strength (MPa)	Elongation at break (%)	Elastic modulus (MPa)
COHP	767.66	170.63	94.51	8.00	6.80	1.01	732.51
CDHP	33.49	157.55	1.36	0.12	1.21	13.68	24.00
UOHP	1027.73	161.83	99.22	8.56	7.13	0.69	978.08
UDHP	182.75	117.21	4.83	0.46	4.06	2.64	196.75

WCA and SFE of COHP, CDHP, UOHP and UDHP coatings were determined in atmospheric environment, and results are shown in Fig. 5a and Table 4. Epoxy resin (EP), Polydimethylsiloxane (PDMS) and Polytetrafluoroethylene (PTFE) were selected as the control samples because they are hydrophobic and also widely used as low surface energy materials. As show in Fig. 5a, the WCA of PDMS and PTFE are 104.5° ± 1.9° and 106.6° ± 3.3°, respectively. The WCAs of COHP, CDHP, UOHP and UDHP coatings are 98.72° ± 1.5°, 110.90 ± 1.5°, 101.5° ± 3.1° and 109.2° ± 2.0°, respectively, indicating that the newly designed polybenzoxazine coatings are also hydrophobic. Obviously, the WCA measurement results suggest that COHP, CDHP, UOHP and UDHP coatings are low surface energy material, as their WCA are higher than 98°. The SFE results also reveal that COHP, CDHP, UOHP and UDHP coatings possesses a low surface energy, the SFEs of COHP, CDHP, UOHP and UDHP coatings are 23.82 ± 0.90 mN/m, 16.59 ± 0.86 mN/m, 22.13 ± 1.89 mN/m and 17.56 ± 1.13 mN/m, respectively. Moreover, CDHP and UDHP have higher contact angles and thus lower surface energies, compared with PDMS and PTFE. In general, low surface energy corresponds to low adhesion force. Therefore, the adhesion force of water on polybenzoxazine coatings and control samples were measured, and results are shown in Fig. 5b. The statistical adhesion force measurement results are shown in Fig. 5c. It can be clearly seen that PDMS and PTFE exhibit relatively low surface adhesion force compared with COHP and UOHP, while CDHP and UDHP reveal lower surface adhesion force than PDMS and PTFE. This result is consistent with the WCA measurement results. The reason for this phenomenon is that the CDHP and UDHP contains octadecylamine structure, which is a highly hydrophobic long alkyl segment, and improves the hydrophobicity of CDHP and UDHP coatings, thereby decreased the surface adhesion force of the CDHP and UDHP coatings.

3.4. Fouling-resistant assays of polybenzoxazine coatings

To examine the antifouling performance of polybenzoxazine coatings, the fouling release performance of polybenzoxazine coatings were determined using typical Gram-negative bacteria *E. coli* (BW25113), Gram-positive bacteria *S. aureus* (ATCC 25923) and marine bacterial *V. alginolyticus* (ATCC 33787). In order to determine the level of biofilm formation on the surface of coatings, the adhesion of bacteria on the surface of polybenzoxazine coatings was visually examined by FE-SEM. Fig. 6 **a-c** respectively shows the SEM image of the three kinds of bacteria: *E. coli*, *S. aureus* and marine bacterial *V. alginolyticus*, attached to COHP, CDHP, UOHP and UDHP coatings. It is easily found that a large number of bacteria were observed on the control group sample made of BG and the bacteria were tightly adhered to the surface of BG, and the distribution was very dense, indicating that it is very susceptible to bacterial adhesion. For COHP and UOHP, compared with BG, the amount of bacterial adhesion has been significantly reduced, but there are still some bacteria on the surface, proving that UOHP and COHP coatings have limited bacteria-resistant properties for *E. coli*, *S. aureus* and marine bacterial *V. alginolyticus*. However, there is almost no bacterial adhesion on the CDHP and UDHP coatings surface, indicating that CDHP and UDHP coatings have better anti-bacterial adhesion properties. Such results are attributed to the low surface energy and low modulus of the coatings.

Table 4
The SFE values of polybenzoxazine coatings.

Samples	COHP	CDHP	UOHP	UDHP
SFE value (mN/m)	23.82 ± 0.90	16.59 ± 0.86	22.13 ± 1.89	17.56 ± 1.13

Microalgae are the unwanted colonization on an artificial surface in marine environments because they easily settle on a wide range of surfaces after the marine conditioning biofilm formed. Therefore, microalgae were adopted as a model fouling specie to further investigate the biofouling resistance of the newly designed polybenzoxazine coatings. Fluorescence microscopy was used to observe the adhesion of microalgae on the sample surfaces. Fig. 7a-c show the fluorescence microscopy images of *N. closterium*, *P. tricornutum* and *D. zhan-jiangensis* cells attached to BG, UOHP, UDHP, COHP and CDHP coatings and Fig. 7d show their area coverage on the surface analyzed by the ImageJ software after immerse for 7 days. As shown in the figure, the uniformly brilliant fluorescence intensity indicated that a large number of microalgae had been equably attached on the surface of BG and it is very susceptible to microalgae adhesion. Statistical analysis showed that the coverage of *N. closterium*, *P. tricornutum* and *D. zhan-jiangensis* cells on the surface of BG after 7 days of immersion were 46.16 ± 5.46 %, 39.68 ± 3.95 % and 11.10 ± 4.09 %, respectively. Statistical results show that the coverage of *N. closterium* cells were 12.34 ± 1.42 %, 1.63 ± 0.49 %, 17.19 ± 1.54 % and 3.55 ± 0.99 %, on the surface of COHP, CDHP, UOHP and UDHP, and that values of *P. tricornutum* and *D. zhan-jiangensis* cells were 12.04 ± 2.94 %, 1.06 ± 0.42 %, 12.06 ± 2.30 %, 1.22 ± 0.61 %, and 0.16 ± 0.03 %, 0.04 ± 0.02 %, 0.27 ± 0.22 %, 0.04 ± 0.01 %, respectively, after 7 days of immersion. For COHP and UOHP, many microalgae cells were attached, proving that COHP and UOHP coating have limited microalgae-resistant properties for *N. closterium*, *P. tricornutum* and *D. zhan-jiangensis* cells. However, there were few microalgae cells adhered on the surface of CDHP and UDHP coatings exhibiting better microalgae-resistant properties than COHP and UOHP. Such results are consistent with bacteria-resistant tests, which attributed to the low surface energy and low modulus of the coatings. Since neither BG nor polybenzoxazine coatings does not have the property of inhibiting the proliferation of microalgae cells, the CDHP and UDHP coatings with low surface energy and low modulus reveal better anti-microalgae adhesion properties.

On the basis of these experimental results, a suggested antifouling mechanism for the newly designed polybenzoxazine coatings was proposed, as shown in Scheme 3. Generally, two antifouling strategies are used to effectively control biofouling. One is to kill fouling organisms

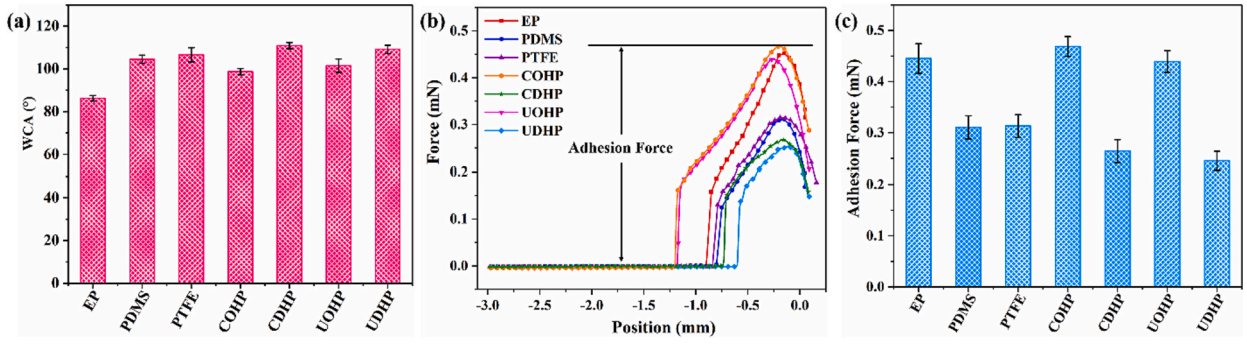

Fig. 5. (a) WCA measurements for polybenzoxazine coatings and control samples in air; (b) adhesion force measurements for polybenzoxazine coatings and control samples; (c) statistical adhesion force measurements for polybenzoxazine coatings and control samples.

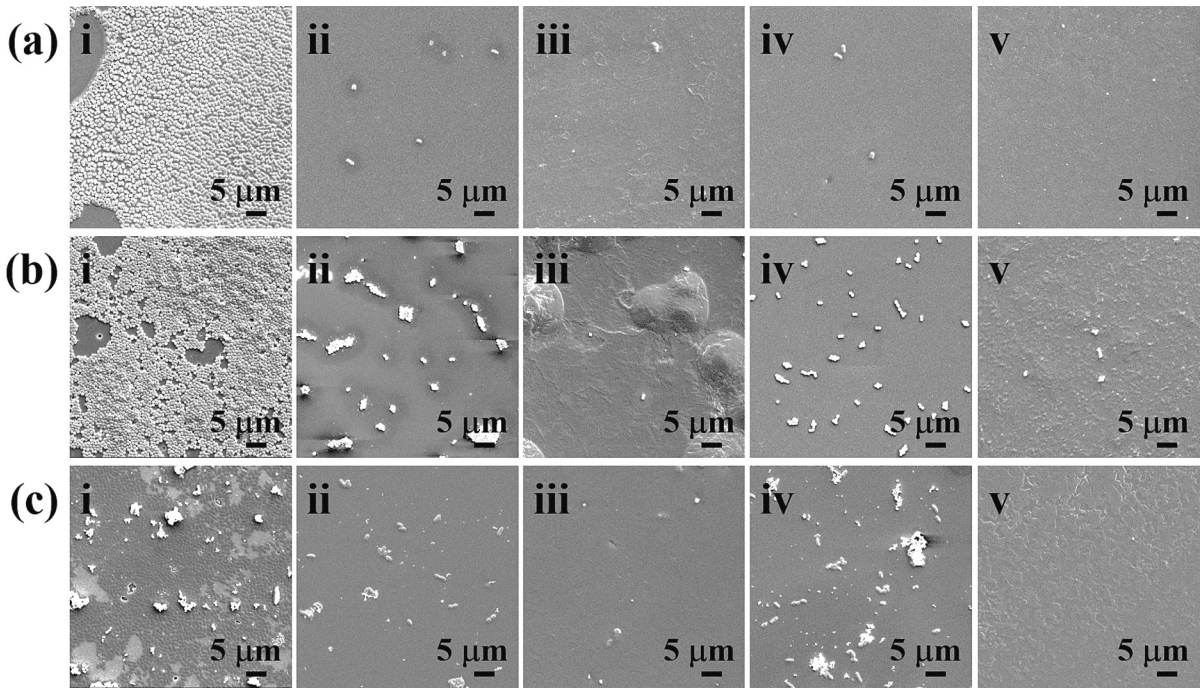

Fig. 6. Adhesion of bacteria (a) *E. coli*, (b) *S. aureus* and (c) *V. alginolyticus* after 24 h of incubation period on surface of (i) BG, (ii) COHP, (iii) CDHP, (iv) UOHP and (v) UDHP coatings by FE-SEM images (the scale bars are 5 μm).

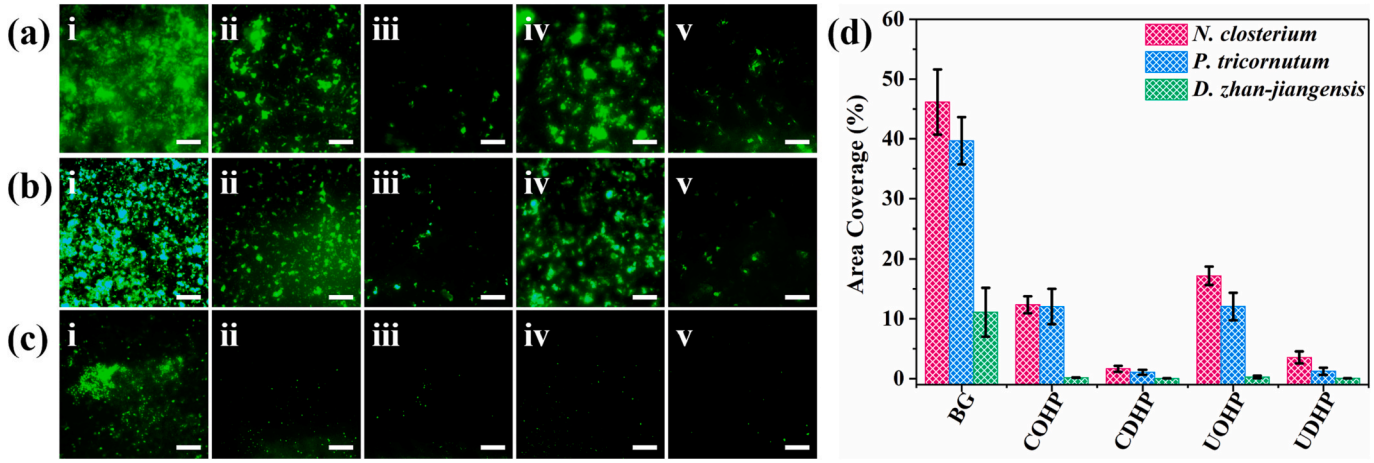

Fig. 7. Fluorescent photographs (0.156 mm^2) of (a) *N. closterium*, (b) *P. tricornutum* and (c) *D. zhan-jiangensis* adhesion after 7 days of cultivation time on (i) BG, (ii) COHP, (iii) CDHP, (iv) UOHP and (v) UDHP coatings (the scale bars are 100 μm); (d) statistical chart showing algal density in examined fields by ImageJ software.

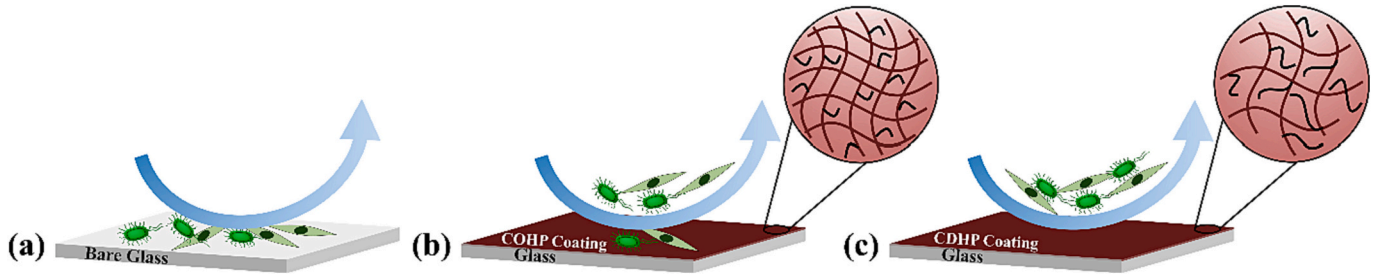

Scheme 3. The suggested antifouling mechanism for the polybenzoxazine coatings, (a) BG, (b) polybenzoxazine synthesized by octylamine, and (c) polybenzoxazine synthesized by octadecylamine.

that are close to or adhere to the surface, relied on the release of toxic antifouling agents in the coating to kill near-fouling organisms or graft antifouling groups on the polymers, to kill near-fouling organisms. Another strategy is fouling release, that is, fouling organisms cannot adhere to the coating or are easily detached when they adhere. For the newly designed polybenzoxazine coatings, there are no toxic antifouling agents or groups effective to kill fouling organisms. Therefore, the antifouling mechanism of the polybenzoxazine coatings mainly depends on the fouling release performance of the low surface energy. Furthermore, the fouling release performance relies on the adhesion of fouling organisms on the coating surface. The weaker the adhesion, the easier it is for the fouling organisms to removal from the coating surface. According to previous literature reports, the adhesion of fouling organisms on the surface of low surface energy coatings is positively correlated with $(E{\cdot}\gamma)^{1/2}$, where E is modulus and γ is surface energy [18,19]. That is, the lower the surface energy, the lower the modulus, and the weaker the adhesion of fouling organisms on the surface of the antifouling coating. For BG, it is a rigid material with high modulus and high surface energy lead to it is very susceptible to fouling organisms (bacteria and microalgae) adhesion, and the adhesion is relatively strong and difficult to remove from the surface. However, through molecular structure design, long and flexible octadecylamine was introduced into the benzoxazine structure, thereby endowing CDHP and UDHP coatings with extremely low surface energy and modulus. The fouling organisms (bacteria and microalgae) adhered weakly to the surface of CDHP and UDHP coatings surface and were easily washed away by PBS, revealed excellent fouling release performance, thus only a few fouling organism adhesions. While COHP and UOHP coatings have relatively low surface energy, but relatively high modulus, because the molecular chain of octylamine is shorter than that of octadecylamine, the adjustment of surface energy and modulus was limited. Therefore, the fouling release performance is limited, and more fouling organisms adhere to the coating surface.

4. Conclusions

A series of natural biomass phenol (cardanol and urushiol)-based benzoxazine monomers with different structures were designed and synthesized by molecular structure design, based on the flexible molecular design of benzoxazine. The difference in structure between urushiol and cardanol, the latent catalytic effect from the presence of a phenolic hydroxyl group on urushiol structure, resulting in a lower activation energy, thereby the ROP temperature of urushiol-based benzoxazine is significantly lower than that of cardanol-based benzoxazine. The properties of polybenzoxazine were further regulated by amine sources with different structures, and the benzoxazine containing octadecylamine with longer carbon chain had higher WCA and lower surface energy. The flexibility of the long carbon chain also effectively reduces the modulus of polybenzoxazine, thus, CDHP and UDHP coatings have lower surface energy and modulus. The fouling organisms have weak adhesion on the low surface energy and low modulus coating surface, thus they are easily washed away by simple water flow, and the CDHP and UDHP coatings show excellent fouling release properties. In this work, the newly designed polybenzoxazine coatings, without any antifoulant, exhibit excellent fouling release performance, which only relies on the low surface energy and low modulus of the coating. This design is a green and eco-friendly antifouling strategy, and provide technical support for the development of eco-friendly antifouling coatings.

CRediT authorship contribution statement

Jipeng Chen: Data curation, Investigation, Methodology, Writing – original draft, Writing – review & editing. **Weibin Bai:** Conceptualization, Methodology, Writing – review & editing. **Rongkun Jian:** Conceptualization, Writing – review & editing, Methodology. **Yucai Lin:** Formal analysis, Methodology, Visualization. **Xiaoxiao Zheng:** Writing – review & editing, Funding acquisition. **Fangfang Wei:** Formal analysis, Resources. **Qi Lin:** Conceptualization. **Fengcai Lin:** Funding acquisition, Validation, Writing – review & editing. **Yanlian Xu:** Conceptualization, Funding acquisition, Methodology, Project administration, Supervision, Writing – review & editing.

Declaration of competing interest

The authors declare that they have no known competing financial interests or personal relationships that could have appeared to influence the work reported in this paper.

Data availability

Data will be made available on request.

Acknowledgements

This work was supported by National Natural Science Foundation of China (grant: 21978050, 32301539), Fujian Province Science and Technology Project: School-Enterprise Cooperation in Science and Engineering (grant: 2020H6029), Marine Economic Development Special Fund Project of Fujian Province (Grant: FUHJF-L-2022-12) and Natural Science Foundation of Fujian Province (Grant: 2022J05234, 2023J011574)

Appendix A. Supplementary data

Supplementary data to this article can be found online at https://doi.org/10.1016/j.porgcoat.2023.108165.

References

[1] H. Jin, J. Wang, L. Tian, M. Gao, J. Zhao, L. Ren, Recent advances in emerging integrated antifouling and anticorrosion coatings, Mater. Design 213 (2022), 110307, https://doi.org/10.1016/j.matdes.2021.110307.
[2] H. Qiu, K. Feng, A. Gapeeva, K. Meurisch, S. Kaps, X. Li, L. Yu, Y.K. Mishra, R. Adelung, M. Baum, Functional polymer materials for modern marine biofouling control, Prog. Polym. Sci. 127 (2022), 101516, https://doi.org/10.1016/j.progpolymsci.2022.101516.
[3] M. Lejars, A. Margaillan, C. Bressy, Fouling release coatings: a nontoxic alternative to biocidal antifouling coatings, Chem. Rev. 112 (2012) 4347–4390, https://doi.org/10.1021/cr200350v.
[4] W.J. Yang, K.-G. Neoh, E.-T. Kang, S.L.-M. Teo, D. Rittschof, Polymer brush coatings for combating marine biofouling, Prog. Polym. Sci. 39 (2014) 1017–1042, https://doi.org/10.1016/j.progpolymsci.2014.02.002.
[5] Q. Xie, J. Pan, C. Ma, G. Zhang, Dynamic surface antifouling: mechanism and systems, Soft Matter 15 (2019) 1087–1107, https://doi.org/10.1039/c8sm01853g.
[6] L. Tian, Y. Yin, W. Bing, E. Jin, Antifouling technology trends in marine environmental protection, J. Bionic Eng. 18 (2021) 239–263, https://doi.org/10.1007/s42235-021-0017-z.
[7] C. Li, M. Atlar, M. Haroutunian, C. Anderson, S. Turkmen, An experimental investigation into the effect of Cu2O particle size on antifouling roughness and hydrodynamic characteristics by using a turbulent flow channel, Ocean Eng. 159 (2018) 481–495, https://doi.org/10.1016/j.oceaneng.2018.01.042.
[8] T.S. Rao, A.J. Kora, P. Chandramohan, B.S. Panigrahi, S.V. Narasimhan, Biofouling and microbial corrosion problem in the thermo-fluid heat exchanger and cooling water system of a nuclear test reactor, Biofouling 25 (2009) 581–591, https://doi.org/10.1080/08927010903016543.
[9] T. Yimyai, R. Thiramanas, T. Phakkeeree, S. Iamsaard, D. Crespy, Adaptive coatings with anticorrosion and antibiofouling properties, Adv. Funct. Mater. 31 (2021), 2102568, https://doi.org/10.1002/adfm.202102568.
[10] I. Fitridge, T. Dempster, J. Guenther, R. de Nys, The impact and control of biofouling in marine aquaculture: a review, Biofouling 28 (2012) 649–669, https://doi.org/10.1080/08927014.2012.700478.
[11] Z. Li, P. Liu, S. Chen, X. Liu, Y. Yu, T. Li, Y. Wan, N. Tang, Y. Liu, Y. Gu, Bioinspired marine antifouling coatings: antifouling mechanisms, design strategies and application feasibility studies, Eur. Polym. J. 190 (2023), 111997, https://doi.org/10.1016/j.eurpolymj.2023.111997.
[12] J. Pan, L. Mei, H. Zhou, C. Zhang, Q. Xie, C. Ma, Self-regenerating zwitterionic hyperbranched polymer with tunable degradation for anti-biofouling coatings, Prog. Org. Coat. 163 (2022), https://doi.org/10.1016/j.porgcoat.2021.106674.
[13] C. Bressy, J.-F. Briand, S. Lafond, R. Davy, F. Mazeas, B. Tanguy, C. Martin, L. Horatius, C. Anton, F. Quiniou, C. Compère, What governs marine fouling assemblages on chemically-active antifouling coatings? Prog. Org. Coat. 164 (2022) https://doi.org/10.1016/j.porgcoat.2021.106701.

[14] A. Turner, Paint particles in the marine environment: an overlooked component of microplastics, Water Res. X 12 (2021), 100110, https://doi.org/10.1016/j.wroa.2021.100110.
[15] Y. Lin, Y. Xie, F. Chen, S. Gong, W. Yang, X. Liang, Y. Lian, J. Chen, F. Wei, W. Bai, Y. Xu, R. Jian, Bioinspired self-stratification fouling release silicone coating with strong adhesion to substrate, Chem. Eng. J. 446 (2022), 137043, https://doi.org/10.1016/j.cej.2022.137043.
[16] P. Hu, Q. Xie, C. Ma, G. Zhang, Silicone-based fouling-release coatings for marine antifouling, Langmuir 36 (2020) 2170–2183, https://doi.org/10.1021/acs.langmuir.9b03926.
[17] J. Chen, R. Jian, K. Yang, W. Bai, C. Huang, Y. Lin, B. Zheng, F. Wei, Q. Lin, Y. Xu, Urushiol-based benzoxazine copper polymer with low surface energy, strong substrate adhesion and antibacterial for marine antifouling application, J. Clean. Prod. 318 (2021), 128527, https://doi.org/10.1016/j.jclepro.2021.128527.
[18] R.F. Brady, I.L. Singer, Mechanical factors favoring release from fouling release coatings, Biofouling 15 (2000) 73–81, https://doi.org/10.1080/08927010009386299.
[19] I.L. Singer, J.G. Kohl, M. Patterson, Mechanical aspects of silicone coatings for hard foulant control, Biofouling 16 (2000) 301–309, https://doi.org/10.1080/08927010009378453.
[20] C. Liu, Q. Xie, C. Ma, G. Zhang, Fouling release property of polydimethylsiloxane-based polyurea with improved adhesion to substrate, Ind. Eng. Chem. Res. 55 (2016) 6671–6676, https://doi.org/10.1021/acs.iecr.6b01003.
[21] C. Liu, C. Ma, Q. Xie, G. Zhang, Self-repairing silicone coatings for marine anti-biofouling, J. Mater. Chem. A 5 (2017) 15855–15861, https://doi.org/10.1039/c7ta05241c.
[22] M.S. Selim, M.A. Shenashen, S.A. El-Safty, S.A. Higazy, M.M. Selim, H. Isago, A. Elmarakbi, Recent progress in marine foul-release polymeric nanocomposite coatings, Prog. Mater. Sci. 87 (2017) 1–32, https://doi.org/10.1016/j.pmatsci.2017.02.001.
[23] J. Chen, J. Zhao, F. Lin, X. Zheng, R. Jian, Y. Lin, F. Wei, Q. Lin, W. Bai, Y. Xu, Polymerized tung oil toughened urushiol-based benzoxazine copper polymer coatings with excellent antifouling performances, Prog. Org. Coat. 177 (2023), 107411, https://doi.org/10.1016/j.porgcoat.2023.107411.
[24] Y. Lu, Y. Zhang, K. Zhang, Renewable biomass resources to access halogen- and phosphorus-free flame retardant thermosets with ultra-low heat release capacity, Chem. Eng. J. 448 (2022), 137670, https://doi.org/10.1016/j.cej.2022.137670.
[25] K. Zhang, X. Yu, Y. Wang, Y. Liu, Thermally activated structural changes of a norbornene–benzoxazine–phthalonitrile thermosetting system: simple synthesis, self-catalyzed polymerization, and outstanding flame retardancy, ACS Appl. Polym. Mater. 1 (2019) 2713–2722, https://doi.org/10.1021/acsapm.9b00668.
[26] X. Wang, H. Niu, J. Huang, L. Song, Y. Hu, A desoxyanisoin- and furfurylamine-derived high-performance benzoxazine thermoset with high glass transition temperature and excellent anti-flammability, Polym. Degrad. Stab. 189 (2021), 109604, https://doi.org/10.1016/j.polymdegradstab.2021.109604.
[27] L. Liu, F. Wang, Y. Zhu, H. Qi, Degradable Schiff base benzoxazine thermosets with high glass transition temperature and its high-performance epoxy alloy: synthesis and properties, Polym. Adv. Technol. 34 (2022) 405–418, https://doi.org/10.1002/pat.5899.
[28] C. Peng, C. Gao, Y. Yuan, Z. Wu, D. Zhou, Synthesis and application of a benzoxazine-type phosphorus-containing monomer on epoxy/benzoxazine copolymer: thermal stability and compatibility with liquid oxygen, Polym. Degrad. Stab. 157 (2018) 131–142, https://doi.org/10.1016/j.polymdegradstab.2018.10.002.
[29] X. Fan, S. Li, C. Wang, Y. Deng, C. Zhang, Z. Wang, Research on fluoropyridine-based benzoxazine with high thermal stability and excellent flame retardancy for its application in coatings, Eur. Polym. J. 187 (2023), 111884, https://doi.org/10.1016/j.eurpolymj.2023.111884.
[30] J. Chen, M. Zeng, Z. Feng, T. Pang, Y. Huang, Q. Xu, Design and preparation of benzoxazine resin with high-frequency low dielectric constants and ultralow dielectric losses, ACS Appl. Polym. Mater. 1 (2019) 625–630, https://doi.org/10.1021/acsapm.8b00083.
[31] L. Zhang, J. Mao, S. Wang, Y. Zheng, X. Liu, Y. Cheng, Benzoxazine based high performance materials with low dielectric constant: a review, Curr. Org. Chem. 23 (2019) 809–822, https://doi.org/10.2174/1385272823666190422130917.
[32] J. Liu, W. Sheng, R. Yang, Y. Liu, Y. Lu, K. Zhang, Synthesis of bio-diamine derived main-chain type benzoxazine resins with low surface free energy, J. Appl. Polym. Sci. 140 (2022), e53578, https://doi.org/10.1002/app.53578.
[33] H. Li, J. Gu, D. Wang, C. Qu, Y. Zhang, Study on benzoxazine-based film adhesive and its adhesion properties with CFPR composites, J. Adhes. Sci. Technol. 31 (2017) 1796–1806, https://doi.org/10.1080/01694243.2017.1283889.
[34] H. Wang, P. Wang, J. Li, Q. Ran, Facile preparation and improved electrochemical performance of oxygen-enriched porous carbon materials based on diacetal-containing polybenzoxazine, Macromol. Mater. Eng. 308 (2022), 2200508, https://doi.org/10.1002/mame.202200508.
[35] W. Xu, H. Wang, Q. Ran, Facile preparation and properties of polybenzoxazine/graphene porous nanocomposites for electromagnetic wave absorption, Polym. Eng. Sci. 62 (2022) 2580–2591, https://doi.org/10.1002/pen.26043.
[36] J. Zong, Q. Ran, Ring opening reaction of 3,4-Dihydro-2H-1,3-Benzoxazine with amines at room temperature, ChemistrySelect 4 (2019) 6687–6696, https://doi.org/10.1002/slct.201901447.
[37] X. Shen, L. Cao, Y. Liu, J. Dai, X. Liu, J. Zhu, S. Du, How does the hydrogen bonding interaction influence the properties of polybenzoxazine? an experimental study combined with computer simulation, Macromolecules 51 (2018) 4782–4799, https://doi.org/10.1021/acs.macromol.8b00741.
[38] M. Selvi, M.R. Vengatesan, S. Devaraju, M. Kumar, M. Alagar, In situ sol–gel synthesis of silica reinforced polybenzoxazine hybrid materials with low surface free energy, RSC Adv. 4 (2014) 8446–8452, https://doi.org/10.1039/c3ra44511a.
[39] M. Monisha, N. Amarnath, S. Mukherjee, B. Lochab, Cardanol benzoxazines: a versatile monomer with advancing applications, Macromol. Chem. Phys. 220 (2018) 1800470, https://doi.org/10.1002/macp.201800470.
[40] G. Mele, G. Vasapollo, Fine chemicals and new hybrid materials from cardanol, Mini-Rev. Org. Chem. 5 (2008) 243–253.
[41] E. Bloise, L. Carbone, G. Colafemmina, L. D'Accolti, S.E. Mazzetto, G. Vasapollo, G. Mele, First example of a lipophilic porphyrin-cardanol hybrid embedded in a cardanol-based micellar nanodispersion, Molecules 17 (2012) 12252–12261, https://doi.org/10.3390/molecules171012252.
[42] A. Minigher, E. Benedetti, O.D. Giacomo, P. Campaner, V. Aroulmoji, Synthesis and characterization of novel cardanol based benzoxazines, Nat. Prod. Commun. 4 (2009) 521–528, https://doi.org/10.1177/1934578X0900400416.
[43] P. Thirukumaran, R. Sathiyamoorthi, A. Shakila Parveen, M. Sarojadevi, New benzoxazines from renewable resources for green composite applications, Polym. Compos. 37 (2014) 573–582, https://doi.org/10.1002/pc.23214.
[44] Y. Cao, C. Chen, X. Lu, D. Xu, J. Huang, Z. Xin, Bio-based polybenzoxazine superhydrophobic coating with active corrosion resistance for carbon steel protection, Surf. Coat. Technol. 405 (2021), https://doi.org/10.1016/j.surfcoat.2020.126569.
[45] Y. Zhao, M. Yuan, L. Wang, X. Lu, Z. Xin, Preparation of bio-based polybenzoxazine/pyrogallol/polyhedral oligomeric silsesquioxane nanocomposites: low dielectric constant and low curing temperature, Macromol. Mater. Eng. 307 (2021), https://doi.org/10.1002/mame.202100747.
[46] L. Wang, M. Yuan, Y. Zhao, Z. Guo, X. Lu, Z. Xin, Fabrication of superhydrophobic bio-based polybenzoxazine/hexagonal boron nitride composite coating for corrosion protection, Prog. Org. Coat. 167 (2022), https://doi.org/10.1016/j.porgcoat.2022.106863.
[47] C. Voirin, S. Caillol, N.V. Sadavarte, B.V. Tawade, B. Boutevin, P.P. Wadgaonkar, Functionalization of cardanol: towards biobased polymers and additives, Polym. Chem. 5 (2014) 3142–3162, https://doi.org/10.1039/c3py01194a.
[48] H. Xu, Z. Lu, G. Zhang, Synthesis and properties of thermosetting resin based on urushiol, RSC Adv. 2 (2012) 2768–2772, https://doi.org/10.1039/c2ra00829g.
[49] A. Ručigaj, R. Ambrožič, M. Krajnc, Thermally assisted self-healing and shape memory behavior of diphenolic acid-based benzoxazines, Macromol. Mater. Eng. 305 (2020), https://doi.org/10.1002/mame.202000463.
[50] X. Li, H. Yao, X. Lu, C. Chen, Y. Cao, Z. Xin, Effect of pyrogallol on the ring-opening polymerization and curing kinetics of a fully bio-based benzoxazine, Thermochim. Acta 694 (2020), https://doi.org/10.1016/j.tca.2020.178787.
[51] B. Hao, J. Wang, Y. Zhang, W. Sheng, K. Zhang, Chrysin-based bio-benzoxazine: a copolymerizable green additive for lowering curing temperatures and improving thermal properties of various thermosetting resins, ACS Appl. Polym. Mater. 4 (2022) 1286–1297, https://doi.org/10.1021/acsapm.1c01679.
[52] Y. Bai, P. Yang, Y. Song, R. Zhu, Y. Gu, Effect of hydrogen bonds on the polymerization of benzoxazines: influence and control, RSC Adv. 6 (2016) 45630–45635, https://doi.org/10.1039/c6ra08881c.
[53] X. Luan, B. Wang, P. Yang, Y. Gu, Enhancing the performances of polybenzoxazines by modulating hydrogen bonds, J. Polym. Res. 26 (2019) 85, https://doi.org/10.1007/s10965-019-1741-5.
[54] K. Zhang, Y. Liu, M. Han, P. Froimowicz, Smart and sustainable design of latent catalyst-containing benzoxazine-bio-resins and application studies, Green Chem. 22 (2020) 1209–1219, https://doi.org/10.1039/c9gc03504d.
[55] M. Zeng, J. Wang, R. Li, J. Liu, W. Chen, Q. Xu, Y. Gu, The curing behavior and thermal property of graphene oxide/benzoxazine nanocomposites, Polymer 54 (2013) 3107–3116, https://doi.org/10.1016/j.polymer.2013.03.069.